Article

TRANSPARENT PROCESS

THE EMBO JOURNAL

Structural insights into mammalian mitochondrial translation elongation catalyzed by mtEFG1

Eva Kummer & Nenad Ban*

Abstract

Mitochondria are eukaryotic organelles of bacterial origin where respiration takes place to produce cellular chemical energy. These reactions are catalyzed by the respiratory chain complexes located in the inner mitochondrial membrane. Notably, key components of the respiratory chain complexes are encoded on the mitochondrial chromosome and their expression relies on a dedicated mitochondrial translation machinery. Defects in the mitochondrial gene expression machinery lead to a variety of diseases in humans mostly affecting tissues with high energy demand such as the nervous system, the heart, or the muscles. The mitochondrial translation system has substantially diverged from its bacterial ancestor, including alterations in the mitoribosomal architecture, multiple changes to the set of translation factors and striking reductions in otherwise conserved tRNA elements. Although a number of structures of mitochondrial ribosomes from different species have been determined, our mechanistic understanding of the mitochondrial translation cycle remains largely unexplored. Here, we present two cryo-EM reconstructions of human mitochondrial elongation factor G1 bound to the mammalian mitochondrial ribosome at two different steps of the tRNA translocation reaction during translation elongation. Our structures explain the mechanism of tRNA and mRNA translocation on the mitoribosome, the regulation of mtEFG1 activity by the ribosomal GTPase-associated center, and the basis of decreased susceptibility of mtEFG1 to the commonly used antibiotic fusidic acid.

Keywords cryo-EM; elongation; mitoribosome; mtEFG1; translation
Subject Categories Structural Biology; Translation & Protein Quality
DOI 10.15252/embj.2020104820 | Received 25 February 2020 | Revised 8 May 2020 | Accepted 11 May 2020 | Published online 30 June 2020
The EMBO Journal (2020) 39: e104820

Introduction

During protein synthesis, the ribosome moves along a messenger RNA (mRNA) that is successively decoded through interactions of mRNA codons with the anticodons of cognate tRNAs on the small ribosomal subunit (SSU). The ribosome harbors three binding sites for tRNAs: the aminoacyl (A) site, the peptidyl (P) site, and the exit (E) site. With the addition of each amino acid, the nascent chain is transferred from the P site-bound tRNA onto the A site tRNA. In a subsequent step, tRNA and mRNA are translocated by exactly one codon on the ribosome leading to a repositioning of the now deacylated P site tRNA to the E site and of the peptidyl-tRNA from the A site to the P site. The deacylated tRNA is then released from the E site of the ribosome, and the ribosomal A site is ready to accept the next aminoacylated tRNA for peptide bond formation (Rodnina, 2018).

The translocation process is an important step during protein synthesis since the fidelity of simultaneous mRNA-tRNA movement has to be very high in order to avoid frameshifting. Indeed, spontaneous frameshifting occurs in < 1 out of 100,000 translated codons demonstrating the high accuracy of the translocation reaction (Kurland, 1992). Translocation requires large-scale movements of the small ribosomal subunit including rotation of the SSU with respect to the large ribosomal subunit (LSU) and a swiveling motion of the SSU head (Ratje *et al*, 2010; Guo & Noller, 2012; Chen *et al*, 2013; Ramrath *et al*, 2013; Tourigny *et al*, 2013; Zhou *et al*, 2013; Holtkamp *et al*, 2014; Belardinelli *et al*, 2016; Wasserman *et al*, 2016). mRNA-tRNA movement occurs in multiple coordinated and evolutionary conserved steps that have been studied in detail in bacteria (for review see Rodnina *et al*, 2019). In the non-rotated ribosome, A and P site tRNAs occupy a "classical" state being bound to the same tRNA site on both SSU and LSU (the tRNA states are therefore denoted A/A and P/P). Subunit rotation triggers movement of the A and P site tRNA to the P and E sites on the LSU while remaining bound to the A and P sites on the SSU (A/ap and P/pe). These tRNA states are referred to as "hybrid" states. Binding of translation elongation factor G stabilizes the rotated ribosome and the hybrid tRNAs to induce the next step of translocation. In this step, movements of head and body of the SSU are uncoupled with the body progressively returning into a non-rotated conformation while the head starts the move, or "swivel", around its own axis. The anticodon stem loops of the tRNAs stay associated with the A and P sites on the SSU head and follow its swiveling motion, which leads to their repositioning into the P and E sites on the SSU body. This tRNA state on the SSU is called "chimeric" (ap/ap and pe/pe). Eventually, the mRNA-tRNA complex is "unlocked", i.e., mRNA-tRNA movement and motions of the SSU head are uncoupled. The acceptor ends of the tRNAs engage with their final positions in the P and E sites on the LSU, respectively, while the SSU head starts to move backwards. The anticodon stem loops (ASLs) of the tRNAs finally

Department of Biology, Institute of Molecular Biology and Biophysics, Swiss Federal Institute of Technology Zurich, Zurich, Switzerland
*Corresponding author. Tel: +41 44 633 2785; E-mail: ban@mol.biol.ethz.ch

© 2020 The Authors

slip into their respective P and E site locations on the SSU head and body adopting again a classical conformation at the end of the translocation reaction (P/P, E/E).

Translocation is catalyzed by elongation factor G (EFG) in bacteria and mtEFG1 in mitochondria, which guide ribosomal motions and tRNA movement (Eberly *et al*, 1985; Chung & Spremulli, 1990; Savelsbergh *et al*, 2003; Bhargava *et al*, 2004; Tsuboi *et al*, 2009; Holtkamp *et al*, 2014; Adio *et al*, 2015). Translocation is possible but very slow in the absence of the elongation factor (Shoji *et al*, 2006; Konevega *et al*, 2007; Bock *et al*, 2013). EFG accelerates the reaction by more than five orders of magnitude (Rodnina *et al*, 1997; Munro *et al*, 2010). As a translational GTPase, it uses the energy derived from GTP hydrolysis to facilitate the rearrangements of the pre-translocation ribosome and tRNA movement (Rodnina *et al*, 1997, 2019; Savelsbergh *et al*, 2003; Holtkamp *et al*, 2014; Adio *et al*, 2015; Belardinelli *et al*, 2016; Chen *et al*, 2016; Sharma *et al*, 2016) by (i) stabilizing the rotated state of the ribosomal subunits, (iii) uncoupling the motions of the SSU head and body from mRNA-tRNA movement during "unlocking", and (iii) likely preventing back slippage of the tRNA during backrotation and backswiveling of the SSU body and head, respectively.

EFG function has been extensively studied in bacteria. However, in the mitochondrial system translation elongation is poorly investigated so far and no structural information is available for mtEFG1 action during mRNA-tRNA translocation on mitochondrial ribosomes. Strikingly, mitochondria have evolved two paralogues of EFG, mtEFG1 and mtEFG2, which catalyze different steps of the translation cycle (Hammarsund *et al*, 2001; Tsuboi *et al*, 2009). Mitochondrial EFG1 (mtEFG1) acts during translation elongation while mitochondrial EFG2 (mtEFG2) partakes in ribosome recycling (Chung & Spremulli, 1990; Bhargava *et al*, 2004; Tsuboi *et al*, 2009). This strict task sharing is in stark contrast to canonical bacterial EFG that plays a role not only in the elongation phase but is also crucially involved in ribosome recycling. The molecular basis for the separation of the dual function of canonical bacterial EFG over two separate proteins in mitochondria is not understood. In recent years, it has become known that also some bacterial species carry two paralogues of EFG (Hammarsund *et al*, 2001; Pandit & Srinivasan, 2003; Atkinson & Baldauf, 2011). However, while both paralogues show a similar task distribution as mitochondrial mtEFG1 and mtEFG2 in the spirochaete Borrelia burgdorferi, the role of EFG2 in other bacterial species is still unclear (Connell *et al*, 2007; Seshadri *et al*, 2009; Suematsu *et al*, 2010).

Here, we employed a previously developed *in vitro* reconstitution system to investigate how mitochondrial mtEFG1 interacts with the mammalian mitoribosome to clarify how mtEFG1 catalyzes tRNA translocation during elongation and how mtEFG1 and mtEFG2 have structurally specialized for their distinct functions.

Results and Discussion

Mitochondrial elongation complexes trapped in two states of translocation

We *in vitro* assembled mitochondrial elongation complexes from isolated, native mammalian *S. scrofa* mitoribosomal subunits, recombinantly generated human mtEFG1 and fMet-mtRNA^{Met} in the presence of a short hexanucleotide (CUGAUG) and the non-hydrolyzable nucleotide analog GMPPNP (please see the Materials and Methods section for details). We find mtEFG1 bound to the factor binding site nestling between the small and large ribosomal subunits. The factor binds the ribosome in an extended fashion and contacts the codon–anticodon paired mRNA-tRNA module in the P site of the ribosome (Fig 1A). Maximum likelihood-based classification approaches yielded two distinct elongation complexes (Figs 1A and EV1 and EV2A and B). Complex 1 (hereafter referred to as POST) at 3.0 Å resembles a post-translocation state carrying a P site tRNA in the classical P/P conformation (Figs 1A and B, and EV2B and EV3A). Complex 2 (hereafter referred to as Ti^{POST}) at 4.2 Å contains two tRNAs that are still in transit into the P and E sites on the SSU showing that our *in vitro* system is in principle translocation competent (Figs 1A and B, and EV2A). In Ti^{POST}, the acceptor ends of both tRNAs already engage with their final positions in the P and E sites on the LSU, respectively, whereas the anticodon stem loops on the SSU are bound in chimeric ap or pe positions, respectively, due to a rotation of the SSU head of about 17° (Fig 1C). Therefore, Ti^{POST} adopts a conformation (ap/P, pe/E) prior to unlocking and shows a similar overall structure as previously reported for translocation intermediates in the bacterial system (Ramrath *et al*, 2013; Tourigny *et al*, 2013; Zhou *et al*, 2014). In Ti^{POST}, the aminoacylated ap/P fMet-tRNA^{Met} contacts the canonical P site element A430 (A790 in *T. thermophilus*) of the SSU body, whereas the P site element of the SSU head, the G782/A783 (G1338/A1339 in *T. thermophilus*) ridge, is still engaged with the deacylated pe/E tRNA^{Met} (Fig 2A) (Selmer *et al*, 2006; Jenner *et al*, 2010). Mutations in G1338/A1339 result in a significant decrease in translational activity in bacteria (Abdi & Fredrick, 2005). Our data show that these rRNA residues have maintained their critical role in mitochondria in guiding the deacylated tRNA into the chimeric pe position on the SSU. Both tRNAs maintain base pairing interactions with their mRNA codons in Ti^{POST}, although the pe/E site tRNA interacts due to a mismatch of the CUG mRNA codon more weakly (Fig 2B). During transition of Ti^{POST} to POST, it appears that upon backswiveling of the SSU head a generally conserved β-hairpin of uS7m will dislodge the deacylated E site tRNA from the mRNA (Fig 2B). The tRNA then engages into the classical E/E position and is eventually ejected from the ribosome.

The conformation of mtEFG1 on the mitochondrial ribosome

The overall conformation of mtEFG1 is similar to previous structural reports from the bacterial system (Fig EV3B) (Agrawal *et al*, 1998; Stark *et al*, 2000; Connell *et al*, 2007; Gao *et al*, 2009; Chen *et al*, 2013; Pulk & Cate, 2013; Ramrath *et al*, 2013; Tourigny *et al*, 2013; Zhou *et al*, 2013; Li *et al*, 2015; Lin *et al*, 2015; Mace *et al*, 2018). The factor is bound to the mitochondrial ribosome in Ti^{POST} and POST states in an extended conformation, where the GTPase (G) domain is bound to the sarcin–ricin loop (SRL) and domain II contacts the SSU body. Domain IV interacts with the mRNA-tRNA codon–anticodon pair of the translocated P site tRNA in Ti^{POST} as well as POST. Domain V of mtEFG1 engages closely with the GTPase-associated center (GAC) on the LSU, and domain III serves as bridging element that stabilizes the domain arrangement of

 © 2020 The Authors

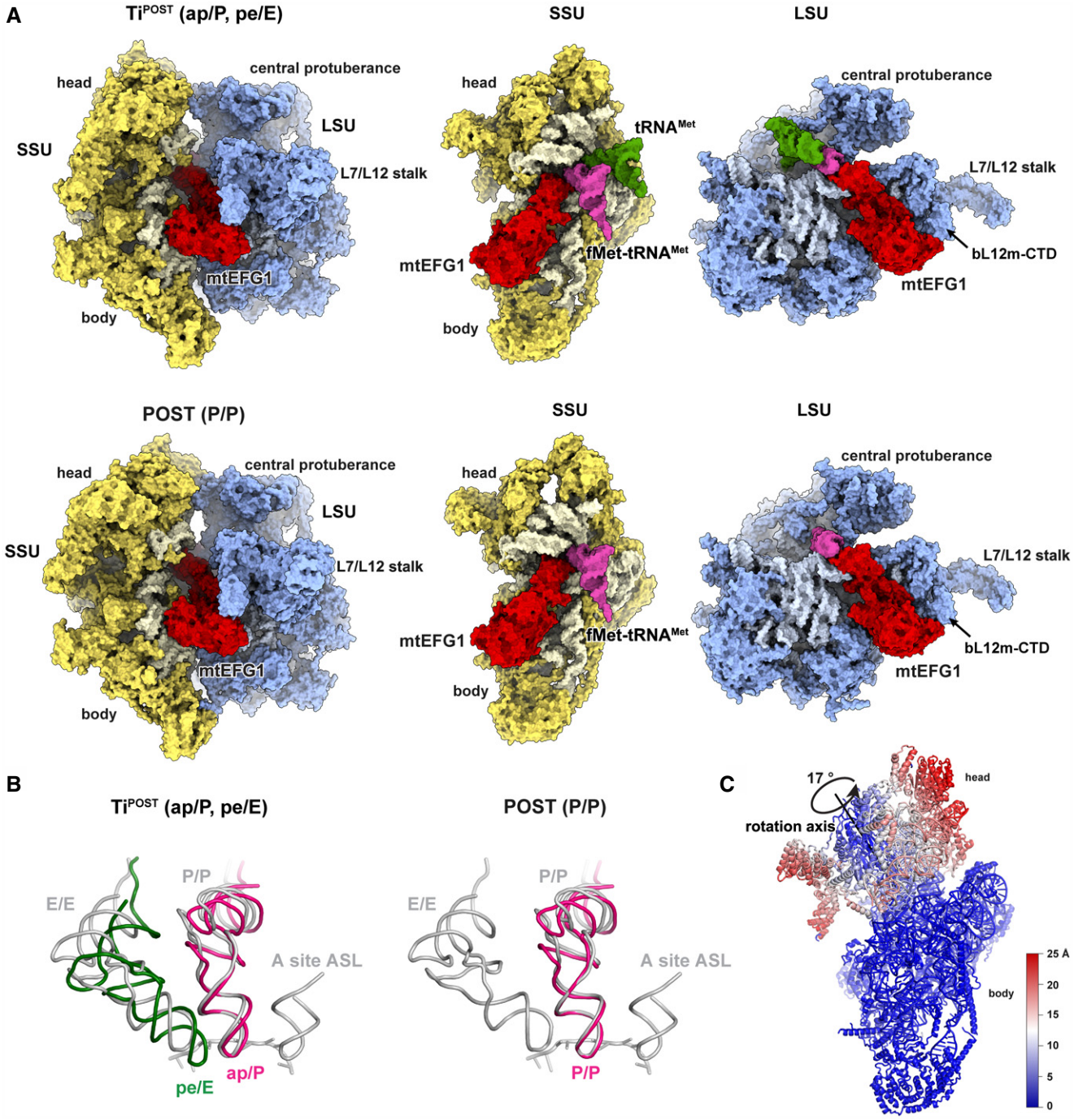

Figure 1. The mitochondrial elongation complex trapped in two states.

A Structures of mtEFG1 (red), aminoacylated fMet-tRNA^{Met} (pink), and deacylated tRNA^{Met} (green) with the 55S mitoribsome in Ti^{POST} and POST states. Separate views for SSU and LSU as seen from the subunit interface are shown for clarity.

B The tRNA orientations of Ti^{POST} and POST are depicted in comparison with published classical tRNA positions (gray) after superposition of the LSU (Selmer *et al*, 2006). The aminoacylated fMet-tRNA^{Met} is colored in pink and the deacylated tRNA^{Met} in green.

C The degree of head rotation comparing the Ti^{POST} and POST complex is shown with the respective rotation axis and angle calculated in PyMOL using the draw_rotation_axis.py script (P.G. Calvo). The resulting displacement in Å is color-coded.

mtEFG1 by simultaneously contacting the G domain and domains II and V (Figs 2D and EV3B).

During translocation, A and P site tRNAs move together with their respective mRNA codons. It has been shown that bacterial EFG is crucial to maintain the mRNA-tRNA interaction during tRNA movement, as the absence or mutation of EFG leads to increased frameshifting and decreased translocation efficiency (Martemyanov *et al*, 1998; Savelsbergh *et al*, 2000a; Holtkamp *et al*, 2014; Peng

© 2020 The Authors

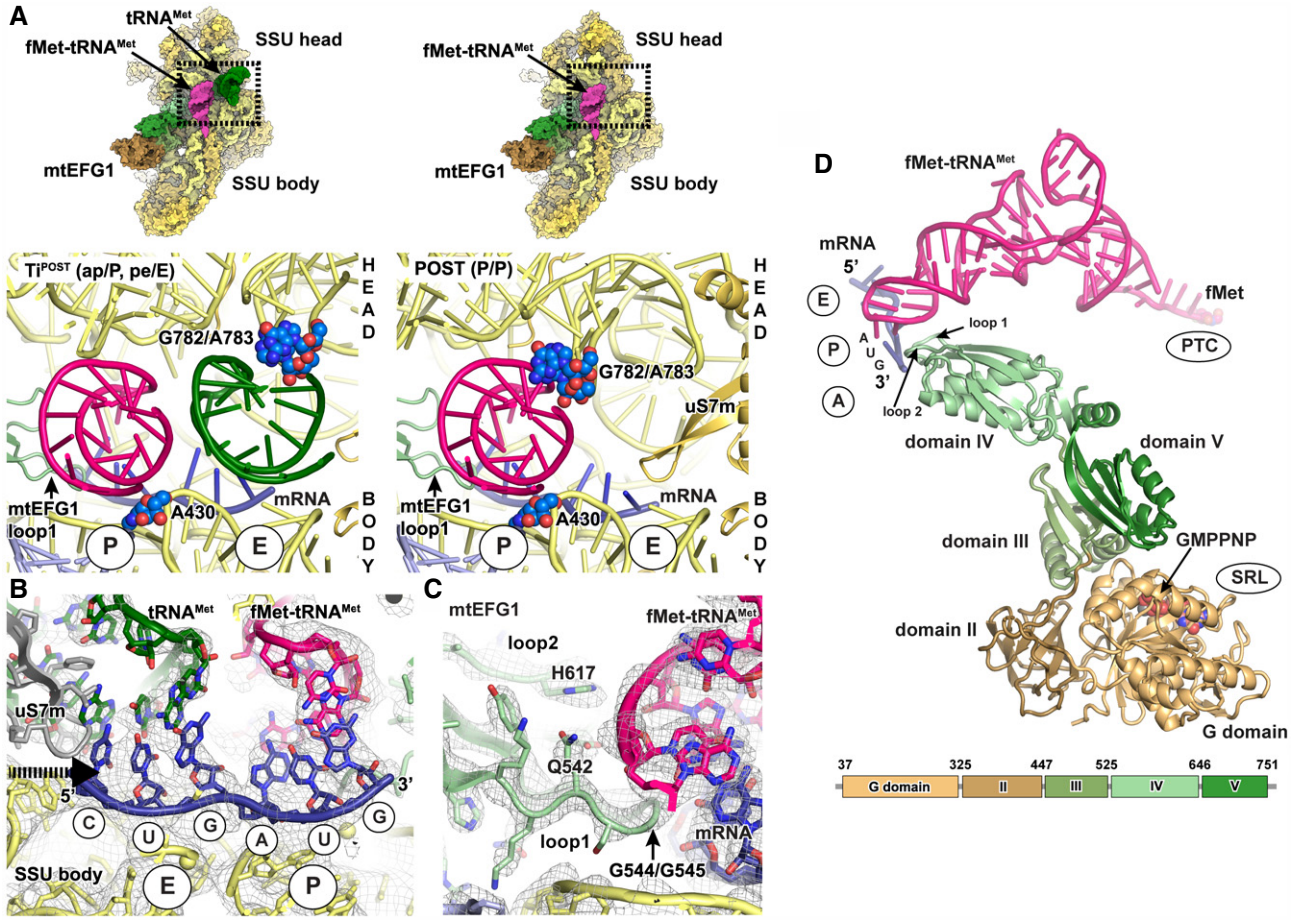

Figure 2. mtEFG1 and tRNA interactions in both translocation states.

A Interactions of the tRNAs in Ti^{POST} and POST states with ribosomal P site elements (blue) of the SSU head (G782/A783 ridge) and body (A430) rRNA. tRNA binding sites of the SSU body are indicated in circles. View from the subunit interface onto the SSU with the enlarged area being highlighted with a box. Left: In the transit Ti^{POST} state, the SSU head is rotated with the G782/A783 ridge moving in concert with deacylated tRNA^{Met} (green). This leads to a repositioning of aminoacylated fMet-tRNA^{Met} and deacylated tRNA^{Met} into a chimeric ap or pe positions, respectively. Right: In the POST state, the aminoacylated fMet-tRNA^{Met} (pink) in the P site engages with both head and body elements.

B Both tRNAs remain associated with their respective mRNA codons in the Ti^{POST} state. A superposition of the position of the uS7m beta-hairpin in the unrotated SSU head conformation is displayed in gray to indicate its clash with the deacylated tRNA^{Met} (green) upon backswiveling of the SSU head. The arrow indicates the direction of motion of uS7m. The EM density of the Ti^{POST} state is contoured at 4σ.

C Loops 1 and 2 of mtEFG1 domain IV contact the fMet-tRNA^{Met}-mRNA module via conserved residues including a di-glycine motif (G544/G545), Q542 and H617 to prevent slippage of the tRNA and to maintain the mRNA reading frame. The EM density and the structural model are shown for the POST state but are very similar in the Ti^{POST} state (The map is depicted at 4σ).

D mtEFG1, fMet-tRNA^{Met}, and mRNA of the POST state are shown in isolation. The domain organization of mtEFG1 is indicated by different colors. A corresponding schematic representation including the amino acid numbering of domain borders is given at the bottom. Locations of the surrounding ribosomal elements are indicated.

et al, 2019; Zhou *et al*, 2019). An important parameter to maintain the mRNA reading frame is the interaction of mtEFG1 domain IV with the tRNA-mRNA module via two apical loops that engage with the minor groove of the codon–anticodon base pairs and with the backbone of the peptidyl-tRNA (Gao *et al*, 2009). This interaction is conserved in mitochondrial translocation as mtEFG1 retained a critical di-glycine motif (G544/G545) at the tip of loop1 that enables the loop to sterically fit into the minor groove of the mRNA-tRNA module (Figs 2C and EV3C). Loops 1 and 2 in addition contain conserved residues Q542 and H617 (Q500 and H573 in *T. thermophilus*) that contact the tRNA backbone and prevent tRNA slippage (Figs 2C and EV3C) (Gao *et al*, 2009; Ramrath *et al*, 2013; Zhou *et al*, 2014; Peng *et al*, 2019).

GTPase regulation of mtEFG1 by ribosomal elements

Translational GTPases engage on the ribosome with several conserved rRNA and protein elements that are important for factor binding and GTPase activation. This GTPase-associated center (GAC) comprises (i) the sarcin–ricin loop (SRL) of the mitochondrial 16S LSU rRNA, (ii) the ribosomal L7/L12 stalk composed of uL10m and 6 copies of bL7/12m in mammalian mitochondria (Kummer

 © 2020 The Authors

et al, 2018), and (iii) the stalk base (SB) that contains uL11m and 16S rRNA helices H43 and H44. In bacteria, the SB is the binding site for antibiotics of the thiopeptide family including thiostrepton that acts as a potent inhibitor of EFG-catalyzed translocation (Harms *et al*, 2008). Accordingly, mutations of the conserved apical adenosine nucleotides A1067 (A512 in *S. scrofa* mitoribosomes) and A1095 (U539 in *S. scrofa* mitoribosomes) of H43 and H44, respectively, confers resistance to thiostrepton in bacteria (Thompson *et al*, 1988; Rosendahl & Douthwaite, 1994; Cameron *et al*, 2004). As mitochondrial H43 harbors an uracil (U539) instead of the conserved adenosine at the tip of H43, mammalian mitoribosomes are naturally resistant to thiostrepton action (Rosendahl & Douthwaite, 1994).

Thiostrepton is believed to act in bacteria not by inhibiting initial EFG engagement with the ribosome but rather by preventing the conversion of a loosely bound initial EFG complex to a stable complex that is competent to catalyze tRNA movement (Rodnina *et al*, 1999; Seo *et al*, 2006; Pan *et al*, 2007; Lin *et al*, 2015). It likely does so by inhibiting movements of the flexible SB that appear to be essential for the conversion into the tight conformation (Schuwirth *et al*, 2005; Harms *et al*, 2008). Rearrangements of the SB upon EFG binding have been observed in the bacterial as well as eukaryotic system although direction and magnitude of the described motions differ (Agrawal *et al*, 1998; Frank & Agrawal, 2001; Spahn *et al*, 2004; Seo *et al*, 2006; Brilot *et al*, 2013; Chen *et al*, 2013; Li *et al*, 2015). Eventually, tight complex formation is accompanied by the establishment of multiple conserved interactions of domain V of the elongation factor with the SB in both systems (Spahn *et al*, 2004; Connell *et al*, 2007; Gao *et al*, 2009; Zhou *et al*, 2013; Lin *et al*, 2015).

In mitochondria, domain V of mtEFG1 closely associates with the GTPase-associated center of the mitoribosome in a manner similar to bacterial EFG (Fig 3). Intriguingly, mtEFG1 binding to the GAC triggers a concerted and directed downward motion of the SB including 16S rRNA H43, H44 as well as uL11m by on average 5 Å (Fig 3B and C). This movement is restricted to the SB as surrounding ribosomal elements are unaffected by factor binding (Fig 3C). SB motion results in a closure of the GAC on domain V of mtEFG1 establishing a large network of interactions that can be roughly clustered into 5 areas tightly connecting the SRL, uL11m-NTD, 16S rRNA helices H43, H44, and H89, and mtEFG1 domain V (Fig 3D and E). Considering that bacterial EFG becomes translocation competent upon conversion from a weakly to a tightly bound state, it is thus tempting to speculate that the observed closure of the mitoribosomal stalk base onto domain V of mtEFG1 may facilitate the progression to the tightly bound conformation. The rearrangement of the GAC appears to be factor-specific as we fail to detect similar motions either in the mitochondrial translation initiation complex containing mitochondrial initiation factor 2 (mtIF2) or in the mitochondrial ribosome in the absence of a translational GTPase (Figs 3B and EV4A) (Greber *et al*, 2015; Kummer *et al*, 2018). Sandwiching of mtEFG1 domain V between the SB and SRL could serve to stabilize the orientation of the G domain and its catalytic motifs at the SRL in order to promote efficient GTP hydrolysis and to delay subsequent release of inorganic phosphate (Fig 3D and E). These observations may be generally applicable to explain why EFG differs in its mode of action from other translational GTPases. Translational GTPases are usually active in the GTP-bound form and use the energy of GTP hydrolysis to leave the ribosome. However, EFG exerts translocation activity in the post-hydrolysis GDP-Pi state as GTP hydrolysis is much faster than tRNA repositioning (Rodnina *et al*, 1997; Savelsbergh *et al*, 2000b, 2003; Seo *et al*, 2006; Belardinelli *et al*, 2016). Closure of the GAC around mtEFG1 domain V and a subsequent stabilization of the G domain on the SRL could be an EFG-specific means to prolong the lifetime of the active GDP-Pi state and to prevent premature dissociation of the factor.

In addition to SB rearrangement, we find a monomer of the bL12m-CTD associated with the G′ subdomain of the mtEFG1 G domain (Figs 3A and EV4A and B). The C-terminal domains (CTDs) of bL12m are mobile elements of the ribosomal L7/L12 stalk, and their function is not fully understood. The bacterial bL12-CTD has been assigned multiple roles in promotion of factor binding, GTPase activation, as well as Pi release (Savelsbergh *et al*, 2000b, 2005; Mohr *et al*, 2002; Diaconu *et al*, 2005). Interactions of the mitochondrial bL12m-CTD have already been observed with the G domain of mtIF2 during translation initiation (Kummer *et al*, 2018). Binding occurs in both cases via a highly conserved surface on the bL12m-CTD but different sites are used on the G domains of mtEFG1 and mtIF2, as the G′ insertion is not present in mtIF2 (Fig EV4A) (Helgstrand *et al*, 2007; Gao *et al*, 2009). It has been reported that *E. coli* EFG is unable to support translocation on mitochondrial ribosomes and this inability was attributed to an incompatibility of the mitochondrial bL12m-CTD with bacterial EFG (Denslow & O'Brien, 1979; Eberly *et al*, 1985; Terasaki *et al*, 2004). However, we do not find bL12m-CTD to engage with mtEFG1 in a different manner as compared to the bacterial system (Gao *et al*, 2009; Tourigny *et al*, 2013; Zhou *et al*, 2013). As the interaction surface of the bL12m-CTD is in addition highly conserved, it remains to be clarified whether and how the bL12m-CTD selects against bacterial translation elongation factor in mitochondrial translation (Fig EV4B and C).

Decreased susceptibility of mtEFG1 to fusidic acid is likely caused by an insertion in switch 1

Fusidic acid (FA) is an antibiotic that is used to treat bacterial infections of the skin or methicillin-resistant *S. aureus* (MRSA) in the clinics. It targets bacterial EFG by binding to an interdomain pocket between the G domain and domain III. Here, it inhibits translation by preventing conformational changes in EFG after GTP hydrolysis and Pi release leading to a trapping of EFG-GDP on the ribosome (Bodley & Lin, 1970; Gao *et al*, 2009). FA binding requires loosening of the catalytically important switch 1 loop of the EFG G domain, as FA would sterically clash with switch 1 at its binding site (Gao *et al*, 2009). Switch 1 is conserved in all translational GTPases and senses the nucleotide state via coordination of a Mg^{2+} ion and two water molecules with the β- and γ-phosphates of the bound GTP molecule.

Strikingly, the translocation activity of mtEFG1 has been shown to be markedly less susceptible to FA than its bacterial counterpart, requiring a 10- to 100-fold higher concentration for FA action (Chung & Spremulli, 1990; Bhargava *et al*, 2004). In accordance, using FA at concentrations similar to the ones that prevent dissociation of bacterial EFG from the ribosome, we do not see mtEFG1 trapped on the mitochondrial ribosome in presence of GTP in our *in vitro* reconstitution system (Ramrath *et al*, 2013). A likely explanation for FA insensitivity is that FA simply fails to bind mtEFG1 at these concentrations (0.5 mM FA + 1 μM mtEFG1) to exert its

© 2020 The Authors

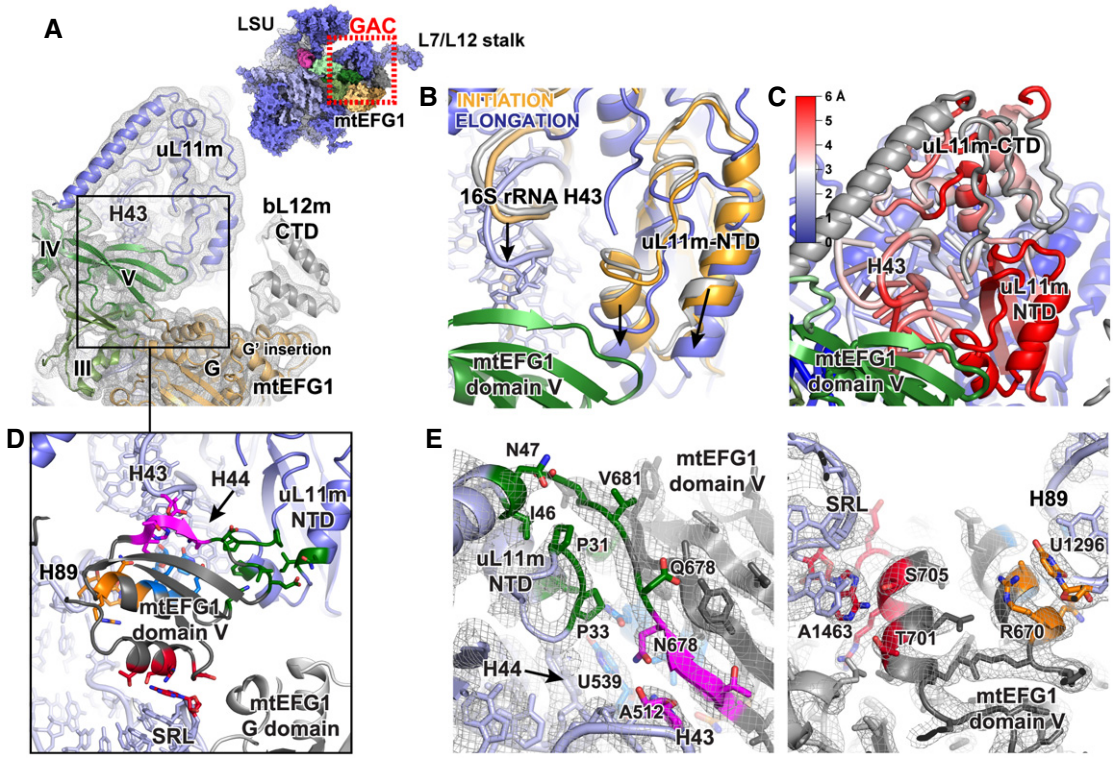

Figure 3. mtEFG1 binding induces a concerted motion in the stalk base of the ribosomal GTPase-associated center.

A The interaction of mtEFG1 in the POST state with the GTPase-associated center (GAC) *via* domain V and with a bL12m-CTD monomer (gray) *via* the G domain are shown (view from the subunit interface onto the LSU). The respective area is highlighted on the inset as red box. mtEFG1 domains are indicated according to the color code introduced in Fig 2D. The corresponding EM density is depicted low-pass filtered to 5 Å and at σ = 2.5.

B The positions of the uL11m N-terminal domain (NTD) and 16S rRNA helices H43 and H44 that form the stalk base of the GAC experience a downward motion upon binding of mtEFG1 (violet) but not upon binding of mtIF2 (orange, pdb: 6GAW; Kummer *et al*, 2018) or in the factor-free ribosome (gray, pdb: 5AJ4 Greber *et al*, 2015). Complexes have been superimposed using the 16S rRNA of the LSU. The arrows display the direction of motion.

C The magnitude of the downward motion of the stalk base comparing the mtIF2-bound and mtEFG1-bound mitoribosome has been calculated in Å, and the stalk base components have been colored accordingly. Elements rebuilt in the current model were excluded from the calculation and are shown in gray.

D An enlarged view of the area in the black box of Fig 3A is shown. mtEFG1 domain V extensively interacts with multiple elements of the GAC at 5 sites that have been color-coded. The orange, pink, and blue clusters interact with 16S rRNA helices H89, H43 and H44, respectively. The red cluster stacks onto the tip of the sarcin–ricin loop (SRL), and the green cluster contacts the uL11m N-terminal domain (NTD).

E Close-ups of the five interaction sites of mtEFG1 domain V with the SRL (red), uL11m-NTD (green), 16S rRNA helices H43 (magenta), H44 (blue), and H89 (orange). The respective EM densities of the POST state are shown at σ = 4.

inhibitory function, and therefore, the factor undergoes a functional GTPase cycle and dissociates from the ribosome. Interestingly, many residues lining the binding pocket of FA are conserved in mtEFG1 including residues that have been shown to confer resistance to FA in the bacterial system upon mutation (Fig 4A, B) (Hansson *et al*, 2005; Gao *et al*, 2009; Ticu *et al*, 2011). Therefore, differences in the primary sequence of mtEFG1 are unlikely to cause the different susceptibility of the bacterial and mitochondrial factors (Bhargava *et al*, 2004). Based on our structure, we propose an alternative explanation for FA resistance due to an increased stabilization of switch 1 in mtEFG1 (Atkinson & Baldauf, 2011). In our reconstructions, we find that the density for switch 1 is very well defined in contrast to a number of reports on bacterial ribosome-bound EFGs that either lack switch 1 density or report conflicting switch 1 conformations in the presence of non-hydrolyzable GTP analogues (Fig 4C) (Chen *et al*, 2013; Pulk & Cate, 2013; Tourigny *et al*, 2013; Zhou *et al*, 2014; Li *et al*, 2015; Lin *et al*, 2015). The reason for the apparently higher stability is likely a well-conserved 3 amino acid insertion in switch 1 of mtEFG1 that carries two positively charged lysine residues K80 and K82 (Fig 4B) (Atkinson & Baldauf, 2011). These two lysines form salt bridges with the phosphate backbone of the SRL and probably account for an additional stability of the switch 1 fold, thereby preventing FA from binding in a pocket that only becomes available when switch 1 residues move out of the way (Fig 4C).

Mitoribosome-specific elements compensate for the rigidity of a reduced L1 stalk

In the bacterial and eukaryotic system, tRNA repositioning from the ribosomal P to the E site is facilitated by interactions between the elbow region of the tRNA and the L1 stalk (Valle *et al*, 2003; Spahn *et al*, 2004; Fei *et al*, 2008, 2009; Fischer *et al*, 2010; Ramrath *et al*, 2013; Tourigny *et al*, 2013; Zhou *et al*, 2013; Mohan & Noller, 2017;

 © 2020 The Authors

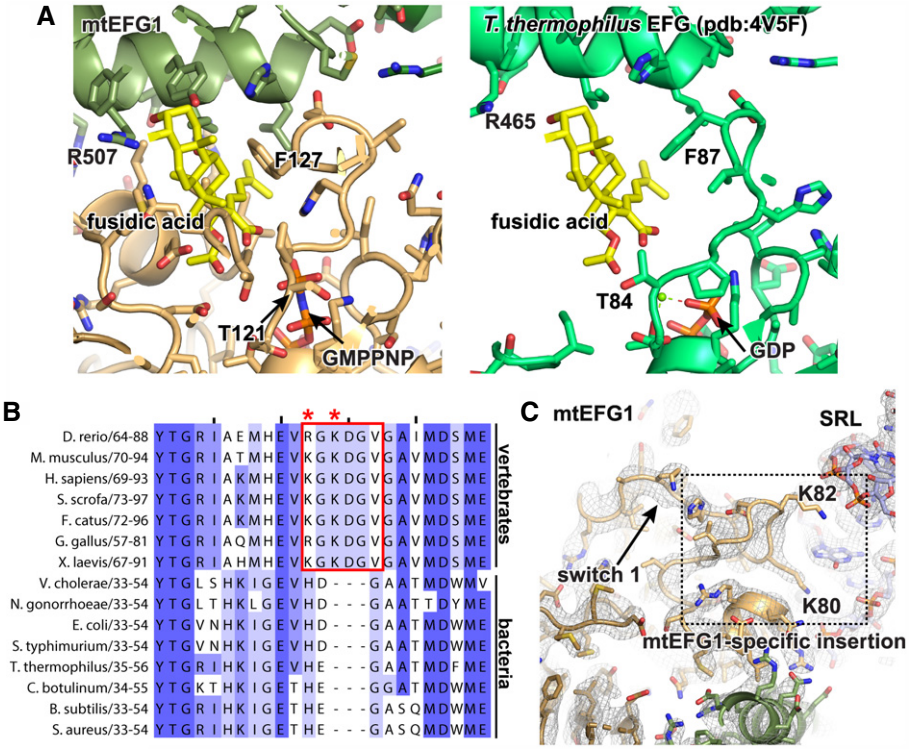

Figure 4. Increased stability of switch 1 may prevent mtEFG1 inhibition by fusidic acid.

A Fusidic acid (yellow) has been modeled into its predicted binding site in mtEFG1 by superimposing a *T. thermophilus* model (pdb: 4V5F Gao *et al*, 2009). Critical residues for FA function are indicated. T121 and G127 correspond to T84 and F87 in *T. thermophilus*. The ordered conformation of switch 1 likely prevents binding of FA to mtEFG1. The bacterial structure, in which FA binding only occurs when switch 1 is disordered, is shown for comparison on the right (pdb:4V5F (Gao *et al*, 2009).

B Clustal Omega sequence alignment of the switch 1 region that contains the mtEFG1-specific insertion from different vertebrate and bacterial species. Coloring was done according to percent identity in Jalview. The insert and K80 and K82 are highlighted with a red box or red asterisks, respectively.

C Switch 1 in the POST state is shown with the corresponding EM density at σ = 4. The position of the mtEFG1-specific insertion with conserved K80 and K82 is boxed.

Mace *et al*, 2018). The L1 stalk is a highly mobile ribosomal element composed of ribosomal RNA and the protein uL1, and its motions have been shown to be correlated with intersubunit rotation and tRNA translocation (Fei *et al*, 2008; Agirrezabala *et al*, 2012; Bock *et al*, 2013; Ning *et al*, 2014). Eventually, transition of the L1 stalk from a closed (inward-facing) to an open (outward-facing)

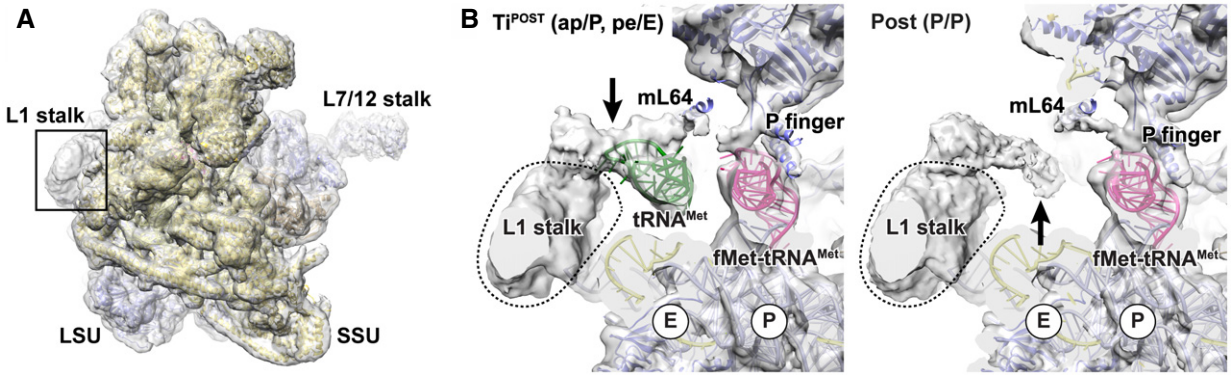

Figure 5. A mitochondria-specific element may compensate for loss of function of the L1 stalk.

A Overview of the POST state to indicate the L1 stalk location (box) on the LSU (violet). The SSU is shown in yellow.

B Close-up of the L1 stalk region on the LSU: EM densities for the Ti^{POST} state and POST state are shown without postprocessing. The position of the immobile L1 stalk is indicated by a dashed line. The mobile element that may replace L1 function is indicated with an arrow. Models for the LSU (violet) as well as aminoacylated fMet-$tRNA^{Met}$ (pink) and deacylated $tRNA^{Met}$ (green) are included.

© 2020 The Authors

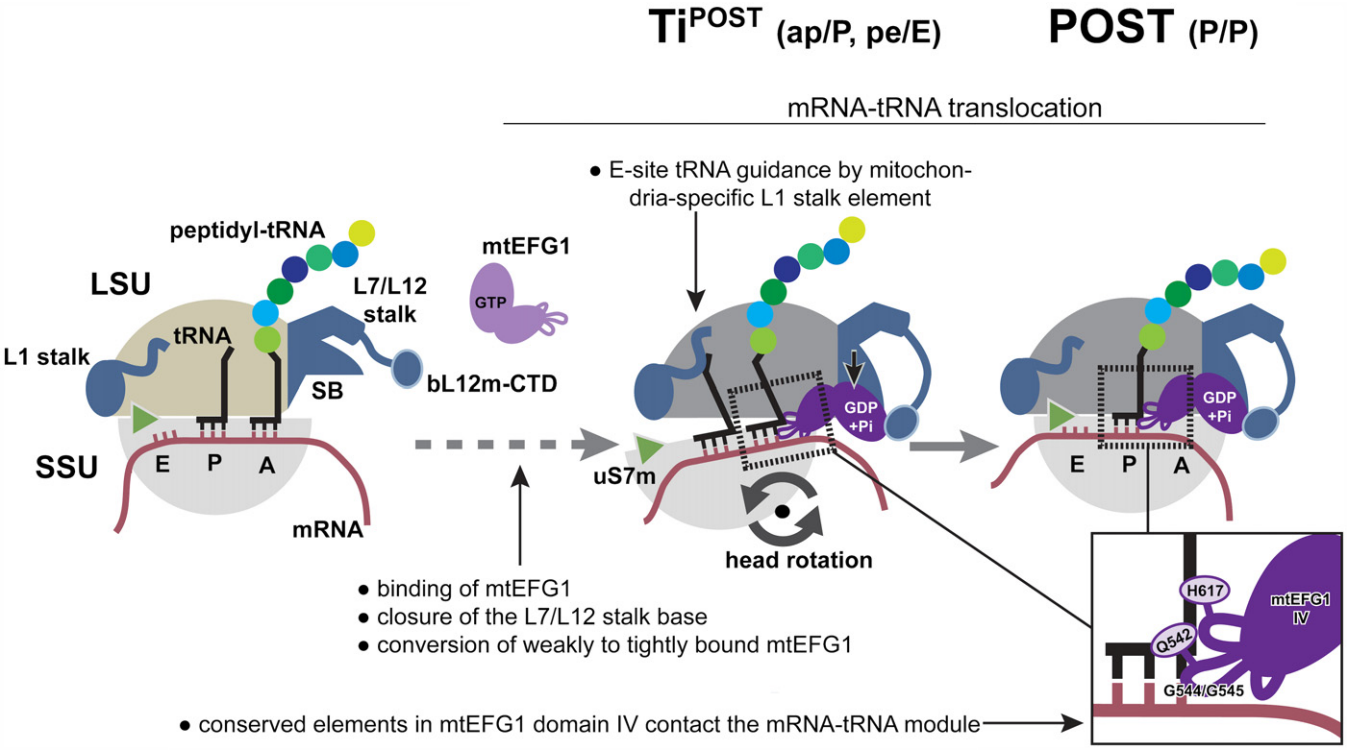

Figure 6. Model for mtEFG1-catalyzed mRNA-tRNA translocation in mammalian mitochondria.
Following peptide bond formation, mtEFG1 is likely recruited to the ribosome by interaction with the bL12m-CTD to catalyze translocation of the mRNA-tRNA module. mtEFG1 binding to the ribosome induces a closure of the L7/L12 stalk base (SB), which converts mtEFG1 from a weakly to a tightly bound state that is translocation competent. Here, closure of the SB may be required to prolong the lifetime of the active GDP-Pi state of mtEFG1. mRNA-tRNA movement depends on large-scale motions of the ribosome. Swiveling of the head repositions the tRNAs on the SSU - the deacylated P site tRNA moves into the chimeric pe position and the peptidyl-tRNA in the A site into the ap position, respectively. Translocation is completed upon backrotation and backswiveling of the SSU body and head, respectively, which positions the peptidyl-tRNA into the classical P/P conformation. mtEFG1 contains highly conserved elements at the tip of domain IV that are required for interaction with the tRNA backbone and the minor groove of the mRNA-tRNA module. Domain IV maintains these contacts throughout the translocation process. The dashed arrow indicates that in analogy to the bacterial system likely multiple additional translocation intermediates exist preceding the ones visualized in this study.

conformation controls ejection of the tRNA from the ribosomal E site at the end of the translocation reaction (Trabuco *et al*, 2010; Ning *et al*, 2014). As a consequence of the evolutionary reduction of rRNA, the mammalian mitochondrial ribosome lacks the 16S rRNA segments (H76/H77) of the L1 stalk that bind the elbow region of tRNAs positioned in the E site of the bacterial and eukaryotic cytosolic ribosomes (Brown *et al*, 2014; Greber *et al*, 2014). Accordingly, the hinge point around which the L1 stalk moves during translocation is not conserved in mitochondria (Reblova *et al*, 2012). This has led to the assumption that the E site tRNA is not stabilized through contacts with the L1 stalk, resulting in a weaker binding to the mitochondrial ribosome (Sharma *et al*, 2003; Brown *et al*, 2014).

Our transit complex now provides information regarding the interaction between a mammalian mitochondrial tRNA and the mitoribosomal E site. In our reconstruction, the L1 stalk indeed does not engage with E site tRNA but remains in a rather static position, presumably due to the absence of a conformationally flexible rRNA hinge point in its base (Fig 5A and B). However, our EM density indicates that the lack of L1 stalk flexibility has been compensated for by a new protein element that emanates from the L1 stalk tip and connects with the mitoribosome-specific P finger (mL40/mL48) and ribosomal protein mL64. We find that this element moves in response to the absence or presence of an E site tRNA and that it contacts the tRNA elbow region in our transit state (Fig 5B). Intriguingly, mammalian mitochondrial tRNAs possess a highly degenerate elbow region that may not permit conventional L1 stalk interactions and whose binding may instead be realized by a mitochondrial-specific element (Sharma *et al*, 2003; Brown *et al*, 2014). Although we could not unambiguously assign the observed density to a protein due to lower resolution of the reconstruction in this area, putative candidate proteins that may contribute to the unknown element are the C-terminus of mL64 or a mitochondrial-specific N-terminal extension of uL1m. Moreover, it is also conceivable that mitoribosomes may have acquired a yet unidentified, additional protein to compensate for loss of L1 functionality. Recently, such an additional protein component, mL108, has for example been identified in the L1 stalk of the fungal mitoribosome (preprint: Itoh *et al*, 2020).

Conclusion

In this work, we present the structures of elongation complexes from mammalian mitochondria at two different steps of the

 © 2020 The Authors

translocation reaction. Our data show that mitochondrial ribosomes translocate the mRNA-tRNA module using conserved motions of the ribosomal small subunit and highly conserved features in mitochondrial elongation factor G1. We find that mtEFG1 does not only control conformational changes in the SSU to promote tRNA movement but also leads to large rearrangements within the GTPase-associated center of the mitochondrial LSU (Fig 6). Our findings imply a mechanism by which mtEFG1 binding leads to closure of the GAC that stabilizes mtEFG1 from a weakly to a tightly bound state that is translocation competent.

We show that the interaction site of mtEFG1 with the mRNA-tRNA module, which serves to maintain the reading frame during translocation, is highly conserved. Strikingly, many of the highly conserved amino acids that recognize the codon–anticodon interacting mRNA/tRNA are absent in the second mitochondrial elongation factor G2, rationalizing why it is unable to promote efficient translocation (Fig EV3C) (Tsuboi *et al*, 2009). Such specialization is possible since a different region of EFG is critical for ribosome recycling in bacteria (Gao *et al*, 2007), and therefore, it appears that mtEFG1 and mtEFG2 become specialized for interaction with the corresponding ligands, mRNA-tRNA in elongation and RRF in recycling, and are no more able to participate in both activities.

We also recognized the role of a mtEFG1-specific insertion in the catalytically important switch 1 region of the G domain and discuss its involvement in the decreased susceptibility of mtEFG1 to the translocation inhibitor fusidic acid. Finally, we have been able to visualize a protein element in the mammalian mitoribosome that appears to compensate for loss of functionality of the otherwise highly conserved ribosomal L1 stalk, which plays a crucial role in translocation and ejection of tRNA in the bacterial and eukaryotic system. In summary, our study provides the structural basis to understand the extent of conservation and diversification of molecular mechanisms that govern mammalian mitochondrial translation elongation. Our data may furthermore aid to rationalize reported mutations in human mtEFG1 that cause combined oxidative phosphorylation deficiency 1 (COXPD1)—a fatal mitochondrial disease leading to early and rapidly progressive hepatoencephalopathy (Coenen *et al*, 2004; Valente *et al*, 2007; Smits *et al*, 2011; Kohda *et al*, 2016).

Materials and Methods

Purification of mtEFG1 and ribosomal subunit

The open reading frame for mtEFG1 was ordered from Thermo Scientific and subcloned into pET24a carrying an N-terminal His_6-tag, a TEV cleavage site and a GGSGSG linker. The protein was expressed in *E. coli* BL21 (DE3) at 18°C overnight. mtEFG1 was affinity purified using a HisTrap FF 5 ml column (GE Healthcare) using standard buffers as described in (Kummer *et al*, 2018). After removal of the His_6-tag upon incubation with TEV-His_6 protease overnight at 4°C, uncleaved mtEFG1, the His_6-tag, and TEV-His_6 protease were removed by reverse Ni^{2+}-based affinity chromatography using a HisTrap FF 5 ml column. Eventually, mtEFG1 was buffer exchanged into storage buffer (40 mM HEPES-KOH pH 7.6, 200 mM KCl, 40 mM $MgCl_2$, 1 mM DTT, 10% (w/v) glycerol) by size exclusion chromatography using a Superdex200 16/600 column (GE Healthcare). Aliquots of mtEFG1 were flash frozen in liquid nitrogen and stored at −80°C until further use. Mitoribosomal subunits were prepared according to published protocols and used for complex formation immediately after purification (Kummer *et al*, 2018).

Preparation of mitochondrial fMet-tRNA^{Met}

Formylated and aminoacylated fMet-tRNA^{Met} was produced following published protocols (Kummer *et al*, 2018). In brief, mitochondrial tRNA^{Met} was generated via run-off T7 transcription and hammerhead ribozyme cleavage. The RNA fragment was purified via agarose gel electrophoresis, folded in the presence of 10 mM $MgCl_2$, aminoacylated and formylated *in vitro,* and purified via phenol-chloroform extraction. Aliquots were flash frozen and stored at −80°C.

Elongation complex formation

Elongation complexes were assembled in 1× monosome buffer (20 mM HEPES-KOH pH 7.6, 100 mM KCl, 40 mM $MgCl_2$, 1 mM DTT, 50 μM spermine) by mixing 60 nM 28S small ribosomal subunit with 1 μM fMet-tRNA^{Met} and 5 μM hexanucleotide (CUGAUG, Microsynth). After incubation for 3 min at 37°C, 60 nM of 39S large ribosomal subunit were added and 55S complex formation was allowed to proceed for 6 more min at 37°C. Subsequently, 1 μM of mtEFG1 premixed with 0.5 mM GMPPNP was added to the mixture and incubated for 3 min at 37°C. The sample was stored at least 10 min on ice before vitrification. The sample was then applied to glow-discharged Quantifoil R2/2 grids coated with a continuous carbon film and vitrified in 1:2 ethane/propane mixture using a Vitrobot Mark IV (FEI).

Of note: The short CUGAUG oligo and mtRNA^{Met} were used for reconstitution due to their efficient binding to the SSU and the elevated propensity of mtRNA^{Met} to bind to the mitoribosomal P site due to a 3× CG base pair in its anticodon stem loop that interacts with the conserved P site G782/A783 ridge. Slightly longer mRNA oligonucleotides were less efficiently bound to the mitoribosomal SSU during *in vitro* reconstitution. Originally, we did not anticipate the non-canonical interaction of the mtRNA^{Met} with the CUG codon in the Ti^{POST} state but it is likely possible due to the tighter binding of the mtRNA^{Met} to the conserved P site elements.

Of note: Swine and human mitochondrial EFG1 are highly similar with 91.7% identity and 96.7% similarity in their primary sequences indicating their strong functional conservation. Therefore, we decided to reconstitute the mammalian mitochondrial translation elongation complex as a chimeric system using porcine mitochondrial ribosomes and human mtEFG1 and fMet-tRNA^{Met} so that the results would be more applicable to the scientist interested in the human system.

Data collection and image processing

Data were collected in movie mode on a FEI Titan Krios equipped with a Falcon III DED (FEI) at 300 kV and a total dose of 40 e-/Å^2. The dose was distributed over 16 frames during a 0.82 s exposure using EPU version 1.9.0.30REL (FEI). Images were recorded at a

© 2020 The Authors

magnification of 100,719× and a defocus range of −0.5 to −2.7 μm. Alignment, summation, and dose weighting of movie frames were done in 5 × 5 patches using MOTIONCOR2 (Grant & Grigorieff, 2015; Zheng *et al*, 2017). CTF estimation was performed in GCTF (Zhang, 2016), and particles were picked using the Laplacian-of-Gaussian function implemented in Relion 3.1 with a minimum particle diameter of 250 Å, a maximum diameter of 350 Å, and a threshold of 0 (Scheres, 2012; Zivanov *et al*, 2018). All further steps were carried out in Relion 3.1 using 4× binned particle images starting with a reference-free 2D classification that yielded 838 311 particles, which underwent subsequent unsupervised 3D classification using the 55S mitoribosome (excluding A and P site tRNAs) as a reference (Greber *et al*, 2015). 55S particles containing clear density for mtEFG1 were selected and 3D autorefined. A mask around mtEFG1 and P site tRNA was applied during the following 3D classification without alignment of particle images to differentiate varying occupancy or conformation of mtEFG1 among the selected particles. The class that displayed the sharpest features for mtEFG1 was selected and further 3D autorefined using unbinned images. After one round of CTF refinement, another 3D classification including the alignment of particle images was done, which unraveled two distinct classes corresponding to POST and Ti^{POST} states. Both classes were 3D autorefined separately. Postprocessing in Relion3.0 yielded a final resolution of 3.0 Å for the POST state and 4.2 Å for the Ti^{POST} state. Please see Fig EV1 for an overview of the particle classification process.

Structure building and refinement

The structures of the 39S large ribosomal subunit, head, and body domains of the 28S small ribosomal subunit as well as fMet-$tRNA^{Met}$ were derived from the 55S initiation complex and fitted separately into the EM densities of the POST or Ti^{POST} states (pdb: 6GAW Kummer *et al*, 2018). A homology model of mtEFG1 was generated from pdb 4WQF (Lin *et al*, 2015) using Phyre2 (Kelley *et al*, 2015) and fitted into the EM densities. Model fitting was performed in UCSF chimera. The models were rebuilt and adjusted in COOT (Emsley *et al*, 2010) to describe the EM densities of both states more accurately. This involved especially mtEFG1, the GTPase-associated center, the decoding center, the central protuberance, and the tRNAs in both states. A homology model of the uL12m-CTD was generated from pdb 1CTF (Leijonmarck & Liljas, 1987) using Phyre2 and fitted into the corresponding density. Manual model building was followed by real-space refinement in PHENIX using default restraints (Ramachandran plot, C-beta deviations, rotamer, secondary structure) and global minimization, as well as B-factor refinement for 5 iterations with a weight between experimental data and restraints of wxc = 1.0 (Afonine *et al*, 2018). For the better-resolved POST state, local rotamer fitting was applied in addition. Resolution estimation (Fig EV5A), particle distribution (Fig EV5B), local resolution plots (Fig EV5C), and the model validation are provided in Fig EV5 and Table EV1, respectively. A list of RNA and protein components of the complexes is provided in Table EV2.

Figure generation

Graphics were generated in PyMOL (Schroedinger), UCSF Chimera or USCF ChimeraX (Pettersen *et al*, 2004; Goddard *et al*, 2018).

Data availability

The cryo-EM density maps have been deposited in the Electron Microscopy Data Bank: accession number EMD-10779 (https://www.ebi.ac.uk/pdbe/entry/emdb/EMD-10779) for the Ti^{POST} state and EMD-10778 (https://www.ebi.ac.uk/pdbe/entry/emdb/EMD-10778) for the POST state. Atomic models have been deposited in the Protein Data Bank (https://www.rcsb.org/): accession number PDB ID 6YDW for the Ti^{POST} state and PDB ID 6YDP for the POST state. Requests for materials should be addressed to N.B. (ban@mol.biol.ethz.ch).

Expanded View for this article is available online.

Acknowledgements
We acknowledge the help of F. Gherlone during mtEFG1 purification, preparation of ribosomal subunits, and initial EM screening. We would like to thank D. Boehringer and S. Mattei for support during EM data acquisition as well as the ScopeM staff for technical support. We are grateful to A. Scaiola for IT support and S. Mattei for discussions. We thank M. Leibundgut for critical reading of the manuscript. We would like to thank D. Ramrath for providing the script to calculate and color code the displacements shown in Figs 1C and 3C. E.K. was supported by an EMBO long-term fellowship (1196-2014). This work was supported by the Swiss National Science Foundation grant (310030B_163478) and via the National Centre of Excellence in RNA and Disease and project funding 138262 to N.B.

Author contributions
Project conceptualization: EK, NB; Sample preparation for EM data collection, data acquisition, calculation of EM reconstructions, building and validation of the structural models, structural data interpretation, figure preparation, and manuscript writing: EK; Structural data interpretation and manuscript revision: NB.

Conflict of interest
The authors declare that they have no conflict of interest.

References

Abdi NM, Fredrick K (2005) Contribution of 16S rRNA nucleotides forming the 30S subunit A and P sites to translation in *Escherichia coli*. *RNA* 11: 1624 – 1632

Adio S, Senyushkina T, Peske F, Fischer N, Wintermeyer W, Rodnina MV (2015) Fluctuations between multiple EF-G-induced chimeric tRNA states during translocation on the ribosome. *Nat Commun* 6: 7442

Afonine PV, Poon BK, Read RJ, Sobolev OV, Terwilliger TC, Urzhumtsev A, Adams PD (2018) Real-space refinement in PHENIX for cryo-EM and crystallography. *Acta Crystallogr D Struct Biol* 74(Pt 6): 531 – 544

Agirrezabala X, Liao HY, Schreiner E, Fu J, Ortiz-Meoz RF, Schulten K, Green R, Frank J (2012) Structural characterization of mRNA-tRNA translocation intermediates. *Proc Natl Acad Sci USA* 109: 6094 – 6099

Agrawal RK, Penczek P, Grassucci RA, Frank J (1998) Visualization of elongation factor G on the *Escherichia coli* 70S ribosome: the mechanism of translocation. *Proc Natl Acad Sci USA* 95: 6134 – 6138

Atkinson GC, Baldauf SL (2011) Evolution of elongation factor G and the origins of mitochondrial and chloroplast forms. *Mol Biol Evol* 28: 1281 – 1292

 © 2020 The Authors

Belardinelli R, Sharma H, Caliskan N, Cunha CE, Peske F, Wintermeyer W, Rodnina MV (2016) Choreography of molecular movements during ribosome progression along mRNA. *Nat Struct Mol Biol* 23: 342 – 348

Bhargava K, Templeton P, Spremulli LL (2004) Expression and characterization of isoform 1 of human mitochondrial elongation factor G. *Protein Expr Purif* 37: 368 – 376

Bock LV, Blau C, Schroder GF, Davydov II, Fischer N, Stark H, Rodnina MV, Vaiana AC, Grubmuller H (2013) Energy barriers and driving forces in tRNA translocation through the ribosome. *Nat Struct Mol Biol* 20: 1390 – 1396

Bodley JW, Lin L (1970) Interaction of *E. coli* G factor with the 50S ribosomal subunit. *Nature* 227: 60 – 61

Brilot AF, Korostelev AA, Ermolenko DN, Grigorieff N (2013) Structure of the ribosome with elongation factor G trapped in the pretranslocation state. *Proc Natl Acad Sci USA* 110: 20994 – 20999

Brown A, Amunts A, Bai XC, Sugimoto Y, Edwards PC, Murshudov G, Scheres SHW, Ramakrishnan V (2014) Structure of the large ribosomal subunit from human mitochondria. *Science* 346: 718 – 722

Cameron DM, Thompson J, Gregory ST, March PE, Dahlberg AE (2004) Thiostrepton-resistant mutants of *Thermus thermophilus*. *Nucleic Acids Res* 32: 3220 – 3227

Chen Y, Feng S, Kumar V, Ero R, Gao YG (2013) Structure of EF-G-ribosome complex in a pretranslocation state. *Nat Struct Mol Biol* 20: 1077 – 1084

Chen C, Cui X, Beausang JF, Zhang H, Farrell I, Cooperman BS, Goldman YE (2016) Elongation factor G initiates translocation through a power stroke. *Proc Natl Acad Sci USA* 113: 7515 – 7520

Chung HK, Spremulli LL (1990) Purification and characterization of elongation factor G from bovine liver mitochondria. *J Biol Chem* 265: 21000 – 21004

Coenen MJ, Antonicka H, Ugalde C, Sasarman F, Rossi R, Heister JG, Newbold RF, Trijbels FJ, van den Heuvel LP, Shoubridge EA *et al* (2004) Mutant mitochondrial elongation factor G1 and combined oxidative phosphorylation deficiency. *N Engl J Med* 351: 2080 – 2086

Connell SR, Takemoto C, Wilson DN, Wang H, Murayama K, Terada T, Shirouzu M, Rost M, Schuler M, Giesebrecht J *et al* (2007) Structural basis for interaction of the ribosome with the switch regions of GTP-bound elongation factors. *Mol Cell* 25: 751 – 764

Denslow ND, O'Brien TW (1979) Elongation factors EF-G from *E. coli* and mammalian mitochondria are not functionally interchangeable. *Biochem Biophys Res Commun* 90: 1257 – 1265

Diaconu M, Kothe U, Schlunzen F, Fischer N, Harms JM, Tonevitsky AG, Stark H, Rodnina MV, Wahl MC (2005) Structural basis for the function of the ribosomal L7/12 stalk in factor binding and GTPase activation. *Cell* 121: 991 – 1004

Eberly SL, Locklear V, Spremulli LL (1985) Bovine mitochondrial ribosomes. Elongation factor specificity. *J Biol Chem* 260: 8721 – 8725

Emsley P, Lohkamp B, Scott WG, Cowtan K (2010) Features and development of Coot. *Acta Crystallogr D Biol Crystallogr* 66(Pt 4): 486 – 501

Fei J, Kosuri P, MacDougall DD, Gonzalez RL Jr (2008) Coupling of ribosomal L1 stalk and tRNA dynamics during translation elongation. *Mol Cell* 30: 348 – 359

Fei J, Bronson JE, Hofman JM, Srinivas RL, Wiggins CH, Gonzalez RL Jr (2009) Allosteric collaboration between elongation factor G and the ribosomal L1 stalk directs tRNA movements during translation. *Proc Natl Acad Sci USA* 106: 15702 – 15707

Fischer N, Konevega AL, Wintermeyer W, Rodnina MV, Stark H (2010) Ribosome dynamics and tRNA movement by time-resolved electron cryomicroscopy. *Nature* 466: 329 – 333

Frank J, Agrawal RK (2001) Ratchet-like movements between the two ribosomal subunits: their implications in elongation factor recognition and tRNA translocation. *Cold Spring Harb Symp Quant Biol* 66: 67 – 75

Gao N, Zavialov AV, Ehrenberg M, Frank J (2007) Specific interaction between EF-G and RRF and its implication for GTP-dependent ribosome splitting into subunits. *J Mol Biol* 374: 1345 – 1358

Gao YG, Selmer M, Dunham CM, Weixlbaumer A, Kelley AC, Ramakrishnan V (2009) The structure of the ribosome with elongation factor G trapped in the posttranslocational state. *Science* 326: 694 – 699

Goddard TD, Huang CC, Meng EC, Pettersen EF, Couch GS, Morris JH, Ferrin TE (2018) UCSF ChimeraX: meeting modern challenges in visualization and analysis. *Protein Sci* 27: 14 – 25

Grant T, Grigorieff N (2015) Measuring the optimal exposure for single particle cryo-EM using a 2.6 A reconstruction of rotavirus VP6. *Elife* 4: e06980

Greber BJ, Boehringer D, Leibundgut M, Bieri P, Leitner A, Schmitz N, Aebersold R, Ban N (2014) The complete structure of the large subunit of the mammalian mitochondrial ribosome. *Nature* 515: 283 – 286

Greber BJ, Bieri P, Leibundgut M, Leitner A, Aebersold R, Boehringer D, Ban N (2015) Ribosome. The complete structure of the 55S mammalian mitochondrial ribosome. *Science* 348: 303 – 308

Guo Z, Noller HF (2012) Rotation of the head of the 30S ribosomal subunit during mRNA translocation. *Proc Natl Acad Sci USA* 109: 20391 – 20394

Hammarsund M, Wilson W, Corcoran M, Merup M, Einhorn S, Grander D, Sangfelt O (2001) Identification and characterization of two novel human mitochondrial elongation factor genes, hEFG2 and hEFG1, phylogenetically conserved through evolution. *Hum Genet* 109: 542 – 550

Hansson S, Singh R, Gudkov AT, Liljas A, Logan DT (2005) Structural insights into fusidic acid resistance and sensitivity in EF-G. *J Mol Biol* 348: 939 – 949

Harms JM, Wilson DN, Schluenzen F, Connell SR, Stachelhaus T, Zaborowska Z, Spahn CM, Fucini P (2008) Translational regulation via L11: molecular switches on the ribosome turned on and off by thiostrepton and micrococcin. *Mol Cell* 30: 26 – 38

Helgstrand M, Mandava CS, Mulder FA, Liljas A, Sanyal S, Akke M (2007) The ribosomal stalk binds to translation factors IF2, EF-Tu, EF-G and RF3 via a conserved region of the L12 C-terminal domain. *J Mol Biol* 365: 468 – 479

Holtkamp W, Wintermeyer W, Rodnina MV (2014) Synchronous tRNA movements during translocation on the ribosome are orchestrated by elongation factor G and GTP hydrolysis. *BioEssays* 36: 908 – 918

Itoh Y, Naschberger A, Martezaei N, Herrmann J, Amunts A (2020) Analysis of translating mitoribosome reveals functional characteristics of protein synthesis in mitochondria of fungi. *bioRxiv* https://doi.org/10.1101/2020.01.31.929331 [PREPRINT]

Jenner LB, Demeshkina N, Yusupova G, Yusupov M (2010) Structural aspects of messenger RNA reading frame maintenance by the ribosome. *Nat Struct Mol Biol* 17: 555 – 560

Kelley LA, Mezulis S, Yates CM, Wass MN, Sternberg MJ (2015) The Phyre2 web portal for protein modeling, prediction and analysis. *Nat Protoc* 10: 845 – 858

Kohda M, Tokuzawa Y, Kishita Y, Nyuzuki H, Moriyama Y, Mizuno Y, Hirata T, Yatsuka Y, Yamashita-Sugahara Y, Nakachi Y *et al* (2016) A comprehensive genomic analysis reveals the genetic landscape of mitochondrial respiratory chain complex deficiencies. *PLoS Genet* 12: e1005679

Konevega AL, Fischer N, Semenkov YP, Stark H, Wintermeyer W, Rodnina MV (2007) Spontaneous reverse movement of mRNA-bound tRNA through the ribosome. *Nat Struct Mol Biol* 14: 318 – 324

Kummer E, Leibundgut M, Rackham O, Lee RG, Boehringer D, Filipovska A, Ban N (2018) Unique features of mammalian mitochondrial translation initiation revealed by cryo-EM. *Nature* 560: 263 – 267

© 2020 The Authors

Kurland CG (1992) Translational accuracy and the fitness of bacteria. *Annu Rev Genet* 26: 29 – 50

Leijonmarck M, Liljas A (1987) Structure of the C-terminal domain of the ribosomal protein L7/L12 from *Escherichia coli* at 1.7 A. *J Mol Biol* 195: 555 – 579

Li W, Liu Z, Koripella RK, Langlois R, Sanyal S, Frank J (2015) Activation of GTP hydrolysis in mRNA-tRNA translocation by elongation factor G. *Sci Adv* 1: e1500169

Lin J, Gagnon MG, Bulkley D, Steitz TA (2015) Conformational changes of elongation factor G on the ribosome during tRNA translocation. *Cell* 160: 219 – 227

Mace K, Giudice E, Chat S, Gillet R (2018) The structure of an elongation factor G-ribosome complex captured in the absence of inhibitors. *Nucleic Acids Res* 46: 3211 – 3217

Martemyanov KA, Yarunin AS, Liljas A, Gudkov AT (1998) An intact conformation at the tip of elongation factor G domain IV is functionally important. *FEBS Lett* 434: 205 – 208

Mohan S, Noller HF (2017) Recurring RNA structural motifs underlie the mechanics of L1 stalk movement. *Nat Commun* 8: 14285

Mohr D, Wintermeyer W, Rodnina MV (2002) GTPase activation of elongation factors Tu and G on the ribosome. *Biochemistry* 41: 12520 – 12528

Munro JB, Wasserman MR, Altman RB, Wang L, Blanchard SC (2010) Correlated conformational events in EF-G and the ribosome regulate translocation. *Nat Struct Mol Biol* 17: 1470 – 1477

Ning W, Fei J, Gonzalez RL Jr (2014) The ribosome uses cooperative conformational changes to maximize and regulate the efficiency of translation. *Proc Natl Acad Sci USA* 111: 12073 – 12078

Pan D, Kirillov SV, Cooperman BS (2007) Kinetically competent intermediates in the translocation step of protein synthesis. *Mol Cell* 25: 519 – 529

Pandit SB, Srinivasan N (2003) Survey for g-proteins in the prokaryotic genomes: prediction of functional roles based on classification. *Proteins* 52: 585 – 597

Peng BZ, Bock LV, Belardinelli R, Peske F, Grubmuller H, Rodnina MV (2019) Active role of elongation factor G in maintaining the mRNA reading frame during translation. *Sci Adv* 5: eaax8030

Pettersen EF, Goddard TD, Huang CC, Couch GS, Greenblatt DM, Meng EC, Ferrin TE (2004) UCSF Chimera–a visualization system for exploratory research and analysis. *J Comput Chem* 25: 1605 – 1612

Pulk A, Cate JH (2013) Control of ribosomal subunit rotation by elongation factor G. *Science* 340: 1235970

Ramrath DJ, Lancaster L, Sprink T, Mielke T, Loerke J, Noller HF, Spahn CM (2013) Visualization of two transfer RNAs trapped in transit during elongation factor G-mediated translocation. *Proc Natl Acad Sci USA* 110: 20964 – 20969

Ratje AH, Loerke J, Mikolajka A, Brunner M, Hildebrand PW, Starosta AL, Donhofer A, Connell SR, Fucini P, Mielke T *et al* (2010) Head swivel on the ribosome facilitates translocation by means of intra-subunit tRNA hybrid sites. *Nature* 468: 713 – 716

Reblova K, Sponer J, Lankas F (2012) Structure and mechanical properties of the ribosomal L1 stalk three-way junction. *Nucleic Acids Res* 40: 6290 – 6303

Rodnina MV, Savelsbergh A, Katunin VI, Wintermeyer W (1997) Hydrolysis of GTP by elongation factor G drives tRNA movement on the ribosome. *Nature* 385: 37 – 41

Rodnina MV, Savelsbergh A, Matassova NB, Katunin VI, Semenkov YP, Wintermeyer W (1999) Thiostrepton inhibits the turnover but not the GTPase of elongation factor G on the ribosome. *Proc Natl Acad Sci USA* 96: 9586 – 9590

Rodnina MV (2018) Translation in prokaryotes. *Cold Spring Harb Perspect Biol* 10: a032664

Rodnina MV, Peske F, Peng BZ, Belardinelli R, Wintermeyer W (2019) Converting GTP hydrolysis into motion: versatile translational elongation factor G. *Biol Chem* 401: 131 – 142

Rosendahl G, Douthwaite S (1994) The antibiotics micrococcin and thiostrepton interact directly with 23S rRNA nucleotides 1067A and 1095A. *Nucleic Acids Res* 22: 357 – 363

Savelsbergh A, Matassova NB, Rodnina MV, Wintermeyer W (2000a) Role of domains 4 and 5 in elongation factor G functions on the ribosome. *J Mol Biol* 300: 951 – 961

Savelsbergh A, Mohr D, Wilden B, Wintermeyer W, Rodnina MV (2000b) Stimulation of the GTPase activity of translation elongation factor G by ribosomal protein L7/12. *J Biol Chem* 275: 890 – 894

Savelsbergh A, Katunin VI, Mohr D, Peske F, Rodnina MV, Wintermeyer W (2003) An elongation factor G-induced ribosome rearrangement precedes tRNA-mRNA translocation. *Mol Cell* 11: 1517 – 1523

Savelsbergh A, Mohr D, Kothe U, Wintermeyer W, Rodnina MV (2005) Control of phosphate release from elongation factor G by ribosomal protein L7/12. *EMBO J* 24: 4316 – 4323

Scheres SH (2012) RELION: implementation of a Bayesian approach to cryo-EM structure determination. *J Struct Biol* 180: 519 – 530

Schuwirth BS, Borovinskaya MA, Hau CW, Zhang W, Vila-Sanjurjo A, Holton JM, Cate JH (2005) Structures of the bacterial ribosome at 3.5 A resolution. *Science* 310: 827 – 834

Selmer M, Dunham CM, Murphy FVT, Weixlbaumer A, Petry S, Kelley AC, Weir JR, Ramakrishnan V (2006) Structure of the 70S ribosome complexed with mRNA and tRNA. *Science* 313: 1935 – 1942

Seo HS, Abedin S, Kamp D, Wilson DN, Nierhaus KH, Cooperman BS (2006) EF-G-dependent GTPase on the ribosome. conformational change and fusidic acid inhibition. *Biochemistry* 45: 2504 – 2514

Seshadri A, Samhita L, Gaur R, Malshetty V, Varshney U (2009) Analysis of the fusA2 locus encoding EFG2 in *Mycobacterium smegmatis*. *Tuberculosis* 89: 453 – 464

Sharma MR, Koc EC, Datta PP, Booth TM, Spremulli LL, Agrawal RK (2003) Structure of the mammalian mitochondrial ribosome reveals an expanded functional role for its component proteins. *Cell* 115: 97 – 108

Sharma H, Adio S, Senyushkina T, Belardinelli R, Peske F, Rodnina MV (2016) Kinetics of spontaneous and EF-G-accelerated rotation of ribosomal subunits. *Cell Rep* 16: 2187 – 2196

Shoji S, Walker SE, Fredrick K (2006) Reverse translocation of tRNA in the ribosome. *Mol Cell* 24: 931 – 942

Smits P, Antonicka H, van Hasselt PM, Weraarpachai W, Haller W, Schreurs M, Venselaar H, Rodenburg RJ, Smeitink JA, van den Heuvel LP (2011) Mutation in subdomain G' of mitochondrial elongation factor G1 is associated with combined OXPHOS deficiency in fibroblasts but not in muscle. *Eur J Hum Genet* 19: 275 – 279

Spahn CM, Gomez-Lorenzo MG, Grassucci RA, Jorgensen R, Andersen GR, Beckmann R, Penczek PA, Ballesta JP, Frank J (2004) Domain movements of elongation factor eEF2 and the eukaryotic 80S ribosome facilitate tRNA translocation. *EMBO J* 23: 1008 – 1019

Stark H, Rodnina MV, Wieden HJ, van Heel M, Wintermeyer W (2000) Large-scale movement of elongation factor G and extensive conformational change of the ribosome during translocation. *Cell* 100: 301 – 309

Suematsu T, Yokobori S, Morita H, Yoshinari S, Ueda T, Kita K, Takeuchi N, Watanabe Y (2010) A bacterial elongation factor G homologue exclusively functions in ribosome recycling in the spirochaete *Borrelia burgdorferi*. *Mol Microbiol* 75: 1445 – 1454

 © 2020 The Authors

Terasaki M, Suzuki T, Hanada T, Watanabe K (2004) Functional compatibility of elongation factors between mammalian mitochondrial and bacterial ribosomes: characterization of GTPase activity and translation elongation by hybrid ribosomes bearing heterologous L7/12 proteins. *J Mol Biol* 336: 331 – 342

Thompson J, Cundliffe E, Dahlberg AE (1988) Site-directed mutagenesis of *Escherichia coli* 23 S ribosomal RNA at position 1067 within the GTP hydrolysis centre. *J Mol Biol* 203: 457 – 465

Ticu C, Murataliev M, Nechifor R, Wilson KS (2011) A central interdomain protein joint in elongation factor G regulates antibiotic sensitivity, GTP hydrolysis, and ribosome translocation. *J Biol Chem* 286: 21697 – 21705

Tourigny DS, Fernandez IS, Kelley AC, Ramakrishnan V (2013) Elongation factor G bound to the ribosome in an intermediate state of translocation. *Science* 340: 1235490

Trabuco LG, Schreiner E, Eargle J, Cornish P, Ha T, Luthey-Schulten Z, Schulten K (2010) The role of L1 stalk-tRNA interaction in the ribosome elongation cycle. *J Mol Biol* 402: 741 – 760

Tsuboi M, Morita H, Nozaki Y, Akama K, Ueda T, Ito K, Nierhaus KH, Takeuchi N (2009) EF-G2mt is an exclusive recycling factor in mammalian mitochondrial protein synthesis. *Mol Cell* 35: 502 – 510

Valente L, Tiranti V, Marsano RM, Malfatti E, Fernandez-Vizarra E, Donnini C, Mereghetti P, De Gioia L, Burlina A, Castellan C *et al* (2007) Infantile encephalopathy and defective mitochondrial DNA translation in patients with mutations of mitochondrial elongation factors EFG1 and EFTu. *Am J Hum Genet* 80: 44 – 58

Valle M, Zavialov A, Li W, Stagg SM, Sengupta J, Nielsen RC, Nissen P, Harvey SC, Ehrenberg M, Frank J (2003) Incorporation of aminoacyl-tRNA into the ribosome as seen by cryo-electron microscopy. *Nat Struct Biol* 10: 899 – 906

Wasserman MR, Alejo JL, Altman RB, Blanchard SC (2016) Multiperspective smFRET reveals rate-determining late intermediates of ribosomal translocation. *Nat Struct Mol Biol* 23: 333 – 341

Zhang K (2016) Gctf: Real-time CTF determination and correction. *J Struct Biol* 193: 1 – 12

Zheng SQ, Palovcak E, Armache JP, Verba KA, Cheng Y, Agard DA (2017) MotionCor2: anisotropic correction of beam-induced motion for improved cryo-electron microscopy. *Nat Methods* 14: 331 – 332

Zhou J, Lancaster L, Donohue JP, Noller HF (2013) Crystal structures of EF-G-ribosome complexes trapped in intermediate states of translocation. *Science* 340: 1236086

Zhou J, Lancaster L, Donohue JP, Noller HF (2014) How the ribosome hands the A-site tRNA to the P site during EF-G-catalyzed translocation. *Science* 345: 1188 – 1191

Zhou J, Lancaster L, Donohue JP, Noller HF (2019) Spontaneous ribosomal translocation of mRNA and tRNAs into a chimeric hybrid state. *Proc Natl Acad Sci USA* 116: 7813 – 7818

Zivanov J, Nakane T, Forsberg BO, Kimanius D, Hagen WJ, Lindahl E, Scheres SH (2018) New tools for automated high-resolution cryo-EM structure determination in RELION-3. *Elife* 7: e42166

© 2020 The Authors